Supporting information

Templating S100A9 amyloids on Aβ fibrillar surfaces revealed by charge detection mass spectrometry, microscopy, kinetic and microfluidic analyses

Jonathan Pansieri,[a#] Igor A. Iashchishyn,[a#] Hussein Fakhouri,[b] Lucija Ostojić,[a] Mantas Malisauskas,[a] Greta Musteikyte,[c] Vytautas Smirnovas,[c] Matthias M. Schneider,[d] Tom Scheidt,[d] Catherine K. Xu,[d] Georg Meisl,[d] Tuomas P. J. Knowles,[de] Ehud Gazit,[a,f] Rodolphe Antoine,[b] Ludmilla A. Morozova-Roche[a]*

---

[a] Jonathan Pansieri, Igor A. Iashchishyn, Lucija Ostojić, Mantas Malisauskas, Ehud Gazit, Ludmilla A. Morozova-Roche
Department of Medical Biochemistry and Biophysics, Umeå University, SE-901 87 Umeå, Sweden

[b] Hussein Fakhouri, Rodolphe Antoine
Institut Lumière Matière UMR 5306, Université Claude Bernard Lyon 1, CNRS, Univ Lyon, F-69100 Villeurbanne, France

[c] Greta Musteikyte, Vytautas Smirnovas
Institute of Biotechnology, Life Sciences Center, Vilnius University, Vilnius, Lithuania

[d] Matthias M. Schneider, Tom Scheidt, Catherine K. Xu, Georg Meisl, Tuomas P. J. Knowles
Centre for Misfolding Diseases, Department of Chemistry, University of Cambridge, Lensfield Road, Cambridge CB2 1EW, United Kingdom

[e] Tuomas P. J. Knowles
Cavendish Laboratory, Department of Physics, University of Cambridge, JJ Thompson Ave, CB3 0HE Cambridge, United Kingdom

[f] Ehud Gazit
School of Molecular Cell Biology and Biotechnology, Tel Aviv University, Tel Aviv 69978, Israel

# Authors with equal contribution

* Corresponding author
E-mail: ludmilla.morozova-roche@umu.se

Materials and methods

Amyloid fibril formation. 0.5 mg of freeze-dried $A\beta_{42}$ peptide (American Peptide Company) was freshly dissolved in distilled water at pH 11.0 and filtered through a 0.22 µm spin membrane filter (Millex, ref. SLGV013SL) to remove any aggregated species. $A\beta_{42}$ fibrils were prepared by incubating 100 µM $A\beta_{42}$ peptide in phosphate buffer saline (PBS, Medicago) at pH 7.4 and 42°C. $A\beta_{42}$ was also subjected to amyloid aggregation in 10 mM HCl buffer at pH 3 and 42°C.

S100A9 protein was expressed in *E.coli* and purified as described previously.[1] Freeze-dried S100A9 was dissolved on ice in PBS buffer at pH 7.4 and 42°C to 400 µM concentration. Before incubation, S100A9 samples were filtered through a 0.22 µm spin membrane filter to remove any aggregates. To conduct experiments at pH 3.0 freeze-dried S100A9 protein was dissolved directly into 10 mM HCl buffer at pH 3 and 42°C.

ThT fluorescence assay. ThT dye is known to bind specifically to β-sheet containing amyloids, and thus enables to follow the kinetics of amyloid self-assembly.[2] $A\beta_{42}$, S100A9 and mixed solutions of $A\beta_{42}$ and S100A9 were prepared at different concentrations on ice, transferred into 96-well plates and then 20 µM ThT was added to each well. The plates were immediately covered, placed into a Tecan F200 PRO plate reader and incubated at 42°C by using 432 rpm orbital shaking every 10 min. ThT fluorescence was also recorded each 10 min, using 450 nm and 490 nm for excitation and emission, respectively. Each sample was incubated in triplicates.

Reaction kinetics fitting. The aggregation kinetics of $A\beta_{42}$-S100A9 co-aggregates and S100A9 were fitted by Amylofit software.[3] Secondary nucleation dominated model was used for $A\beta_{42}$-S100A9 with elongation rate set as a global fitting parameter and critical nuclei size for primary and secondary nucleation was set to 2 ($n_c = n_2 = 2$). Number of basin hops was set to five. By using described parameters, the fitting was performed seven times in order to estimate the accuracy of the fitted values, which is illustrated by the error bars in the corresponding figure. In the fitting of the co-aggregation kinetics, the ThT signal from S100A9 fibrils was neglected, since the ratio of the plateau intensities for

the similar concentrations of S100A9 and $A\beta_{42}$ is much less than 1 ($I_{S100A9}/I_{A\beta} \ll 1$). Nuclear-dependent polymerisation model was used to fit the S100A9 kinetics. Critical nucleus size, n_c, and combined rate constant, $k_n k_+$, were used as global fit parameters.

AFM imaging. 15 µL of each sample were deposited on the surface of mica for 30 min, washed 5 times with 200 µL deionized water and left to dry overnight at room temperature. AFM imaging was performed in a PeakForce QNM mode in air by using a BioScope Catalyst atomic force microscope (Bruker). Resolution was set at 512 x 512 pixels, scan rate was 0.51 Hz, and scan sizes were 2 x 2 and 5 x 5 µm. Bruker RTESPA and SNL cantilevers were used. Heights of amyloid fibrils were measured in the cross-sections by using a Bruker Nanoscope analysis software, while their lengths were measured by using ImageJ software.

AFM size distributions. Histograms of AFM fibril length and cross-sectional height distributions were built up by using the kernel density estimate and resampling techniques. Each distribution was built up by following procedures: firstly, the empirical distribution function was constructed for each observed AFM data set by using Gaussian kernel with bandwidth selected by Wand's method;[4] secondly, the sample size of 10^4 was drawn from each distribution function. Thirdly, the histogram with bin size equal to the above bandwidth was constructed for each data set. This procedure was applied to all experimental data sets. The above resampling procedures did not affect the distribution parameters such as median and its deviation.

CDMS instrument. The CDMS measurements were performed on home-built CDMS instrument in the single pass mode and the RMS detector noise was ~100e. In CDMS, an ion passes through a metal tube. A positive ion entering an isolated conducting tube induces a negative charge on the inner surface and a positive charge on the outside. The induced charges are maintained until the ion exits, at which point they dissipate. The mass-to-charge ratio (*m/z*) of the trapped ion is determined from the time-of-flight (TOF) *Δt*, *i.e.* time delay between the positive and negative pulses that corresponds to the entrance and the exit from the detector tube.

Ion velocity, v_m, is determined as $v_m = \frac{L}{\Delta t}$ and *m/z* ratio is defined as $\frac{m}{z} = \frac{2eV}{v_m^2 - v_g^2}$, where *L = 3.75 cm* is length of the detector tube, *eV=155 V* – electrostatic acceleration voltage and v_g*= 375 m/s* – the ion velocity due to the free gas expansion. Indeed, in our system a correction is needed to take into account the initial kinetic energy imposed on the ion by the free jet expansion of the gas prior to acceleration by the electric field.

Electrospray ionization (ESI) conditions. To enhance ionization efficiencies, 25% methanol was added to all samples of corresponding amyloid fibrils and 22.5 μM final polypeptide concentrations were reached prior injection into the ESI source. The amyloid samples were injected at flow rates of typically 0.2-0.6 mL/h and entered the electrospray chamber through a 0.1 mm internal diameter stainless steel capillary tube located inside the needle tip. Nitrogen gas was injected between the end cap and the transfer glass capillary and was flown through a heater, typically set at 200°C. The vacuum interface was composed of a glass transfer capillary that passes the ions into the first stage of the vacuum system, an end cap, a skimmer between the first and second vacuum stages, a hexapole ion guide and an exit lens. The ESI source generates charged macroions, which are guided by an ionic train to the mass spectrometer. Ions are guided up to a vacuum stage chamber (~5.10^{-6} mbar) and directed through the charge detection device. Importantly, the low charged population of amyloid fibrils was observed here due to improved signal to noise ratio of the home-built CDMS instrument. In our previous studies on amyloid populations we were able to detect only ions with charges higher than ~300 e.[11,12] In the present work, the limit of charges was significantly reduced to ~200 e, due to improvements in the noise level in the pick-up signal and the addition of frequency filters.

CDMS data processing. We used a home-developed Windows-based software to record chromatograms – VISUAL C++. The program calculates the time between the maxima of the positive and negative pulses, the amplitudes of two pulses and the ratio between their absolute values. A high-frequency filter is added to the data processing of traces in order to remove peak artefacts. Residual droplets are excluded by using post-processing

thresholds for TOF (> 95 μs). In this work, only ions with charges higher than ~200 e that both enter and exit the tube, are counted. Events for which the absolute values of the amplitude ratios between the first and the second pulses are greater than 1.5 or less than 0.75 are automatically excluded. Finally, the corresponding ion counting rate ranges around 50 ions/s. For each ion the mass is deduced from its *m/z* and *z* values. For each sample, measured ions were filtered with respect to molecular mass (< 1 GDa) and charge (< 3 ke). Resulting sample sizes used in this study were thus 2863 for $A\beta_{42}$, 839 for S100A9 and 1771 for $A\beta_{42}$-S100A9 sample.

Ranking of amyloid particles according to their CDMS charge to mass ratio (z/m). The values of CDMS *z/m* ratios for each individual ion within each amyloid data set were arranged in descending order. Following the ranking, the positions of individual charged ions were plotted along *x*-axis, while *z/m* ratios were shown along *y*-axis. These values were compared to the *z/m* ratios of $A\beta_{42}$ and S100A9 monomers, calculated based on their amino acid sequences at pH 7.4 by using a ProteinCalculator v.3.4 (protcalc.sourceforge.net).

CDMS data analysis. In order to analyse the data in two dimensions of mass and charge, the joint mass-charge frequency distributions were constructed as shown schematically in Fig. S1 and described below. Firstly, the range of data was binned with respect to charge and mass; secondly, the numbers of ions falling into corresponding bins were counted and thirdly, the counts were divided by the sample size, i.e. total number of ions in the sample. The optimal bin width was calculated for each molecular mass distribution using one level recursive Wand method.[4] Optimal bin width ensures that the histogram is not oversmoothed. The same bin number was used for all samples, i.e. 50 bins. The same number of 50 bins was used for the charge range since molecular mass and charge are dependent quantities.[5]

We have constructed three joint frequency distributions with respect to mass and charge termed as follows: $\Phi(m,z) = \Phi_{A\beta_{42}}$, Φ_{S100A9} and $\Phi_{A\beta_{42}-S100A9}$. Subsequently, difference frequency distributions were constructed by pointwise subtraction:

$\Delta_{A\beta_{42}} = \Phi_{A\beta_{42}-S100A9} - \Phi_{A\beta_{42}}$

$$\Delta_{S100A9} = \Phi_{A\beta_{42}-S100A9} - \Phi_{S100A9}$$ and

$$\Delta_{A\beta_{42}-S100A9} = \Phi_{A\beta_{42}-S100A9} - \Phi_{A\beta_{42}} - \Phi_{S100A9}$$.

Since the range of Φ and Δ spans more than two orders of magnitude, the following logarithmic transformation $\hat{\Omega}$ was used:

$$\hat{\Omega} = \frac{ln(\frac{\Omega}{\Omega_{max}})}{ln(\frac{\Omega_{min}}{\Omega_{max}})},$$

where: Ω denotes either of the following Φ or Δ distributions, $\Omega_{min}, \Omega_{max}$ – minimal and maximal values among three distributions of either $\Phi_{A\beta_{42}}$, Φ_{S100A9} and $\Phi_{A\beta_{42}-S100A9}$ or $\Delta_{A\beta_{42}}$, Δ_{S100A9} and $\Delta_{A\beta_{42}-S100A9}$, respectively. Taking the minimal and maximal values across all three Φ or Δ distributions, respectively, ensures that after the log-transformation samples can be compared. The ranges of the difference distributions Δ are not symmetrical around 0, therefore two log-transformation have been performed separately for negative and positive values. In order to keep scaling symmetrical around 0, the widest range of all Δ was used to select minimal and maximal values for log-transformation. The absolute values were used for log-transformation and minus was assigned for the negative range of the log-transformed Δ values (Fig. S1).

The log-transformed distributions of $\Phi\ and\ \Delta$ are represented by maps, where the colour corresponds to the frequency value. In order to keep the perception of the colour-mapped scalar value (frequency) linear with respect to human eye colour perception, the diverging colour scheme suggested by Moreland[6] was used. It was scaled between 0 to 1 for the log-transformed frequency distributions Φ and between -1 to 1 for the log-transformed difference distributions Δ. We term the corresponding log-transformed frequency distributions as *frequency maps* and log-transformed difference frequency distributions as *difference maps*, respectively (Fig. S1).

Simulated CDMS distribution. Probability mass function (PMF) was used to characterize the distribution of a discrete random variable such as mass. It associates the probability to any given number that the random variable will be equal to that number. We have simulated the molecular mass distribution of the fibril mixture based on CDMS

molecular mass distributions of $A\beta_{42}$ and S100A9 individual samples. In the case of separately formed fibrils the samples can be considered independent in mathematical sense, i.e. PMF of $A\beta_{42}$ fibrillar sample does not depend on the PMF of S100A9 amyloid sample, which is not the case when co-aggregation occurs, i.e. for $A\beta_{42}$-S100A9 amyloid sample. Imposing additional condition that sticking probabilities of fibrils do not depend on the fibril size and their type, we have calculated the distribution of molecular mass of preformed fibril mixture. Then PMF of mixed fibrils is the convolution of PMFs of individual components as follows: if $X = A\beta_{42}$, $Y = S100A9$ and $Z = X + Y$ = $A\beta_{42}$+S100A9, then:

$$PMF_z(z) = PMF_y(z - x)PMF_x(x).$$

Mathematica 12 software was used to make statistical calculations and visualisation of results.

Microfluidic binding assay. The microfluidic binding assay was used here as reported previously.[8-10] Stream of fluorescently labelled analyte was injected from one side in a microfluidic channel alongside with auxiliary buffer flow coming from the opposite side into the channel under laminar flow conditions, allowing mixing by diffusion only (Fig. 5A). By tracking the spatial diffusion of the analyte into the co-flow buffer, the hydrodynamic radius, R_h, was determined. The binding affinity, K_d, and stoichiometry, α, were derived from the changes in R_h by using Bayesian analysis.

The S100A9 protein was fluorescently labelled by incubation with three molar equivalents of Alexa Fluor 647 (ThermoFisher, UK) for 1 h after buffer exchange to $NaHCO_3$ (0.1 M, pH 8.3). The protein conjugate was purified on a Superdex 200 increase 10/30 gL column (GE Healthcare, US) with a flow rate of 0.5 mL/min with PBS as elution buffer, containing 0.02 % NaN_3 (w/v).

$A\beta_{42}$ monomer was purified as reported previously, including a series of purification cycles.[7] For the final purification step monomeric $A\beta_{42}$ was incubated in Gdn-HCl (8 M in sodium phosphate buffer) for 1 h and purified on a Superdex 75 increase 10/30 gL column with sodium phosphate buffer (20 mM, pH 8.0, with 0.2 mM EDTA). $A\beta_{42}$ fibrils were obtained by incubating 30 μM monomeric $A\beta_{42}$ in 20 mM sodium phosphate buffer (pH 8.0, containing 0.2 mM EDTA) at 37°C with double orbital rotation (400 rpm) in a 96-well plate in a FLUOstar OPTIMA plate reader (BMG Labtech). The aggregation of $A\beta_{42}$ was

followed by measuring the fluorescence increase of 20 mM ThT in one similar aliquot. After completion of the aggregation reaction, the fibrils were collected and used in the microfluidic binding assay.

S100A9 was incubated with varying concentration of $A\beta_{42}$ in sodium phosphate buffer and Tween 20 (0.02 % v/v) for 2 h. The increase in size upon binding was detected by applying microfluidic diffusional sizing in Fluidity One W (Fluidic Analytics, Cambridge, UK) series of purification cycles. For the S100A9 protein in absence of $A\beta_{42}$ fibrils a hydrodynamic radius R_h = 2.52 ± 0.13 nm was determined, which is in a good agreement with the theoretically expected radius of 2.46 nm for a dimer of 13,242 Da protein.

Analysis of microfluidic binding data. In our binding equilibrium we have S100A9 (A) and fibrillar Aβ peptide (B):

$$A + B \rightleftharpoons AB$$

$$K_d = \frac{[A][B]}{[AB]}$$

Denoting the total concentrations of A and B as $[A]_0$ and $[B]_0$, respectively, we obtain the following expression for the concentration of A bound to B, $[AB]$:

$$[AB] = \frac{[A]_0 + [B]_0 + K_d - \sqrt{([A]_0 + [B]_0 + K_d)^2 - 4[A]_0[B]_0}}{2}$$

It is important to note that B here denotes the concentration of fibril binding sites, rather than monomers in the fibril. The hydrodynamic radius is calculated from measurements of the fluorescence intensities of the 'diffused' and 'undiffused' channels, termed I_d and I_u, respectively. However, unlike the radius, the fraction of labelled substrate that ends up in the 'diffused' channel, $y = \frac{I_d}{I_d + I_u}$, is easy to relate to the concentration of A bound. We thus describe the analysis here in terms of *y*, while the conversion to R_h can be performed after fitting. We also define the parameters r_f and r_b, denoting the fractions of free and bound labelled substrate, respectively, that are detected in the 'diffused' channel. The following equations describe the intensities in each channel:

$$I_d = \kappa([AB]r_b + ([A]_0 - [AB])r_f)$$

$$I_u = \kappa([AB](1 - r_b) + ([A]_0 - [AB])(1 - r_f)),$$

where κ is a constant relating label concentration with fluorescence intensity detected.

We can therefore express the predicted fraction in the diffused channel by:

$$f_d = \frac{([AB]r_b + ([A]_0 - [AB])r_f)}{[A]_0}$$

with [AB] determined by the equation above. Therefore, the predicted fraction in the diffused channel is a function of r_f, r_b, K_d, $[A]_0$, and $[B]_0$, thus denoted by $f_d(r_f, r_b, K_d, [A]_0, [B]_0)$.

Finally, the stoichiometry, α, of the Aβ fibril : S100A9 (B : A) interactions are also not known. In order to account for this, we define α as the number of S100A9 binding sites per Aβ monomer within the Aβ fibrils, so that $[B]_0 = \alpha[B]_{tot}$ where $[B]_0$ represents the concentration of binding sites, and $[B]_{tot}$ the fibril concentration in terms of monomer equivalents. We assume that the radii of singly or multiply bound fibrils are equal, and that there is no cooperativity in the binding. We therefore have the following expression for $[AB]$:

$$[AB] = \frac{[A]_0 + \alpha[B]_{tot} + K_d - \sqrt{([A]_0 + \alpha[B]_{tot} + K_d)^2 - 4\alpha[A]_0[B]_{tot}}}{2}$$

The expression for the predicted fraction to end up in the diffused channel is therefore $f_d(r_f, r_b, K_d, \alpha, [A]_0, [B]_0)$, where there are 4 unknown parameters, α, r_f, r_b, and K_d. Analysis then proceeds via Bayesian inference. For r_f and r_b we assume the prior is flat in linear space, whereas for the K_d and α a prior, that is flat in logarithmic space, is chosen.

We assume our experimental measurement data to be normally distributed about the true value; our likelihood function is therefore a Gaussian, centered on the theoretical measurement value.

$$P(data|parameters) \propto exp[-\frac{1}{2\sigma^2}\sum_{i=1}^{N}(y_i - f_d(r_f, r_b, K_d, \alpha, [A]_i, [B]_i))^2]$$

where f_d is defined as above, $[A]_i$ and $[B]_i$ are the concentrations of S100A9 binding sites and Aβ, respectively, in the *i*th measurement, and y_i is the fraction of diffused labelled component in the *i*th measurement. In order to define an appropriate standard deviation, σ, for each dataset, we calculate the standard deviations of repeats of each measurement and use the maximum of these values as a global standard deviation for that dataset. Inference is performed by calculation of the 4-dimensional posterior at evenly spaced

points for all parameters, at 50 points each for r_f and r_b, and 100 points each for α and K_d, with ranges chosen such that there is no clear probability mass outside the sampled region. Marginalisation is used to obtain 1-dimensional distributions and thus calculate errors for the parameters.

References

[1] T. Vogl, A. L. Gharibyan and L. A. Morozova-Roche, *Int. J. Mol. Sci.* **2012**, *13*, 2893–2917.
[2] H. Naiki, K. Higuchi, M. Hosokawa and T. Takeda, *Anal. Biochem.* **1989**, *177*, 244–249.
[3] G. Meisl, J. B. Kirkegaard, P. Arosio, T. C. T. Michaels, M. Vendruscolo, C. M. Dobson, S. Linse and T. P. J. Knowles, *Nat. Protoc.* **2016**, *11*, 252–272.
[4] M. P. Wand, *Americ. Stat.* **1997**, *51*, 59–64.
[5] P. Kebarle and U. H. Verkerk, *Mass Spectrom. Rev.* **2009**, *28*, 898–917.
[6] K. Moreland, in *Advances in Visual Computing* (Eds.: G. Bebis, R. Boyle, B. Parvin, D. Koracin, Y. Kuno, J. Wang, R. Pajarola, P. Lindstrom, A. Hinkenjann, M.L. Encarnação, et al.), Springer, Berlin, Heidelberg, **2009**, pp. 92–103.
[7] S. I. A. Cohen, P. Arosio, J. Presto, F. R. Kurudenkandy, H. Biverstål, L. Dolfe, C. Dunning, X. Yang, B. Frohm, M. Vendruscolo, J. Johansson, C. M. Dobson, A. Fisahn, T. P. J. Knowles and S. Linse. Nat. Struct. Mol. Biol. **2015**, 22, 207-213.
[8] P. Arosio, T. Muller, L. Rajah, E. V. Yates, F. A. Aprile, Y. Zhang, S. I. A. Cohen, D. A. White, T. W. Herling, E. J. De Genst, S. Linse, M. Vendruscolo, C. M. Dobson and T. P. J. Knowles, Microfluidic Diffusion Analysis of the Sizes and Interactions of Proteins under Native Solution Conditions. ACS Nano, **2016**, 10, 333–341.
[9] T. Scheidt, U. Lapinska, J. R. Kumita, D. R. Whiten, D. Klenerman, M. R. Wilson, S. I. A. Cohen, S. Linse, M. Vendruscolo, C. M. Dobson, T. P. J. Knowles and P. Arosio, Secondary nucleation and elongation occur at different sites on Alzheimer's amyloid-β aggregates. *Sci. Adv*. **2019**, 5, eaau3112.
[10] S. Linse, T. Scheidt, K. Bernfur, M. Vendruscolo, C. M. Dobson, S. I. A. Cohen, E. Sileikis, M. Lundquist, F. Qian, T. O'Malley, T Bussiere, P. H. Weinreb, C. K. Xu, G. Meisl, S. Devenish, T. P. J. Knowles and O. Hansson. Kinetic fingerprint of antibody therapies predicts outcomes of Alzheimer's clinical trials. **2019**, bioRxiv, doi.org/10.1101/815308.
[11] T. Doussineau, C. Mathevon, L. Altamura, C. Vendrely, P. Dugourd, V. Forge and R. Antoine, *Angew. Chem. Int. Ed. Engl.*, 2016, **55**, 2340–2344.
[12] J. Pansieri, M. A. Halim, C. Vendrely, M. Dumoulin, F. Legrand, M. Moulin Sallanon, S. Chierici, S. Denti, X. Dagany, P. Dugourd, C. Marquette, R. Antoine and V. Forge, *Chem. Sci.*, 2018, **9**, 2791–2796.

Author contribution

J.P., I.A.I. and L.A.M.-R. conceived and designed the work, and wrote the manuscript. J.P. and L.O. performed the *in vitro* characterizations of the amyloid fibrillation. H.F. and R.A. conceived, performed and analysed CDMS experiments. I.A.I. conducted conceptualization, formal analysis, methodology, validation and visualisation. M.M.S. and T.S. performed microfluidic experiments; the binding and kinetic analyses were conducted by C.K.X., G.M. and T.P.J.K. M.M., G.M. and V.S. prepared polypeptide samples. J.P., I.A.I., E.G. and L.A.M.-R. coordinated all experiments and compiled the results. All co-authors discussed and commented on the manuscript.

Supplementary figures

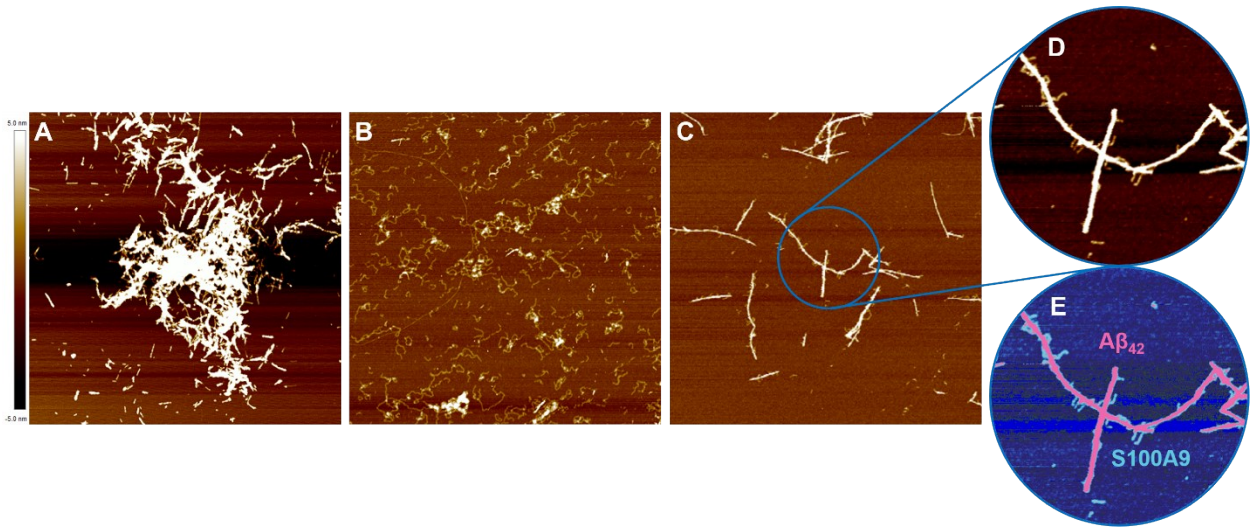

Figure S1. AFM analysis of $A\beta_{42}$, S100A9 and co-aggregated $A\beta_{42}$-S100A9 amyloids. AFM images of amyloids of (A) 30 μM $A\beta_{42}$, (B) 30 μM S100A9 and (C) $A\beta_{42}$-S100A9 (30 μM $A\beta_{42}$ and 5 μM S100A9 were co-incubated). Amyloids were formed after 24 h incubation in PBS, pH 7.4, 42°C. Scan sizes are 5 x 5 μm. (D,E) Magnified images of $A\beta_{42}$ fibrils with S100A9 amyloids templated on their surfaces presented in arbitrary colour scheme.

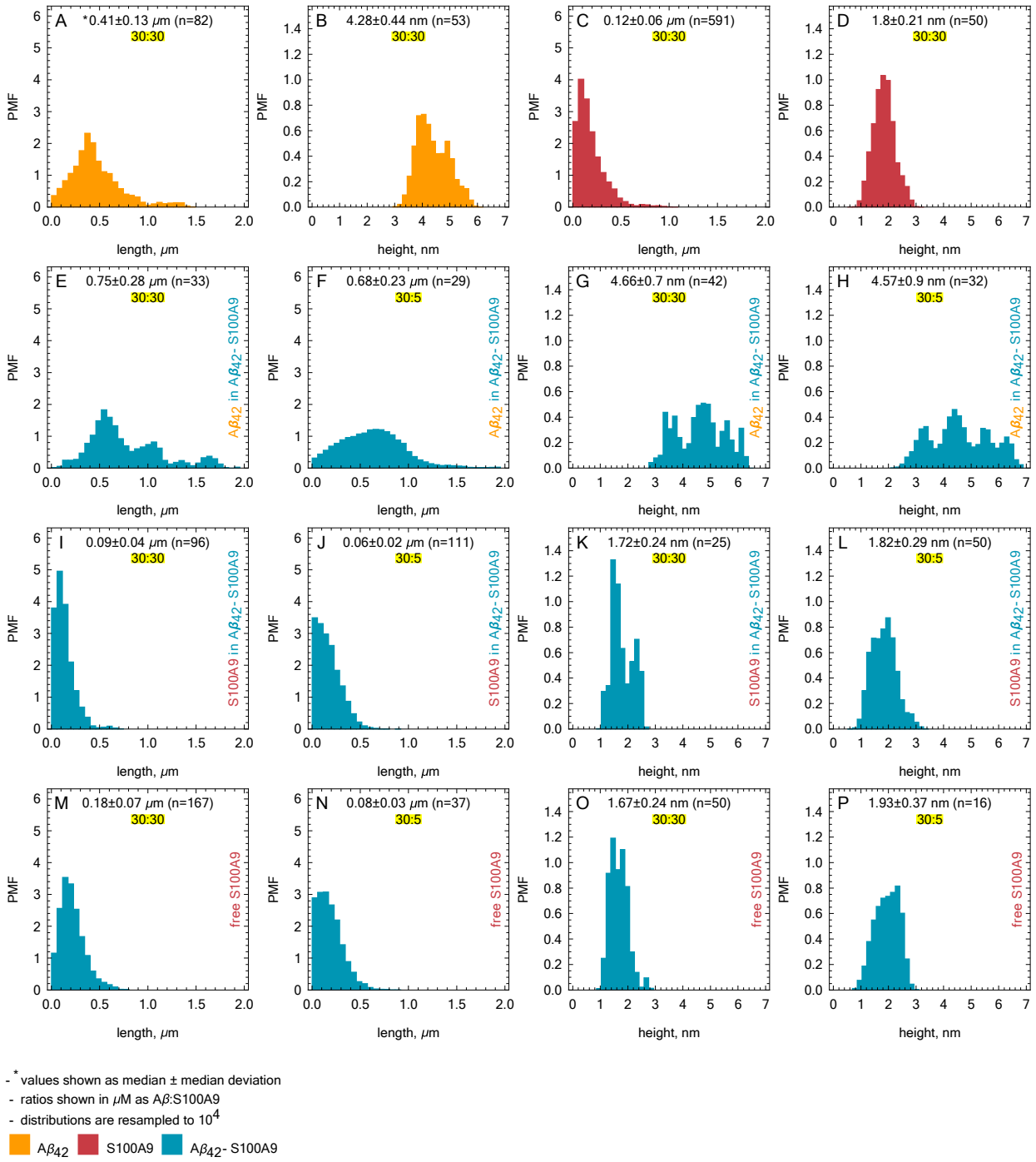

Figure S2. Length and height distributions of amyloid fibrils measured by AFM. Length of fibrils were measured by ImageJ software. The heights of amyloid fibrils were measured by Bruker Nanoscope analysis software in the AFM cross-sections. Probability mass function (PMF) defined as probability of finding fibril with specific length or height is indicated along *y*-axes. The measured values of lengths or heights are indicated along *x*-axes. The length and height distributions for $A\beta_{42}$ fibrils are shown in yellow, for S100A9 fibrils – in red and for $A\beta_{42}$-S100A9 amyloids – in blue. The distributions for $A\beta_{42}$ fibrils within $A\beta_{42}$-S100A9 complexes are shown in 3rd row; for thin S100A9 fibrils templated on the surfaces of $A\beta_{42}$-S100A9 complexes – in 4th row and for free S100A9 in the $A\beta_{42}$-S100A9 samples in 5th row. The molar ratios of $A\beta_{42}$ and S100A9 co-incubated

in $A\beta_{42}$-S100A9 samples are shown in each figure legends as 30:30 or 30:5, respectively. *The median values of corresponding distributions and sample sizes are also shown in each figure. The distributions are resampled to 10^4 (See ESI Material and Methods).

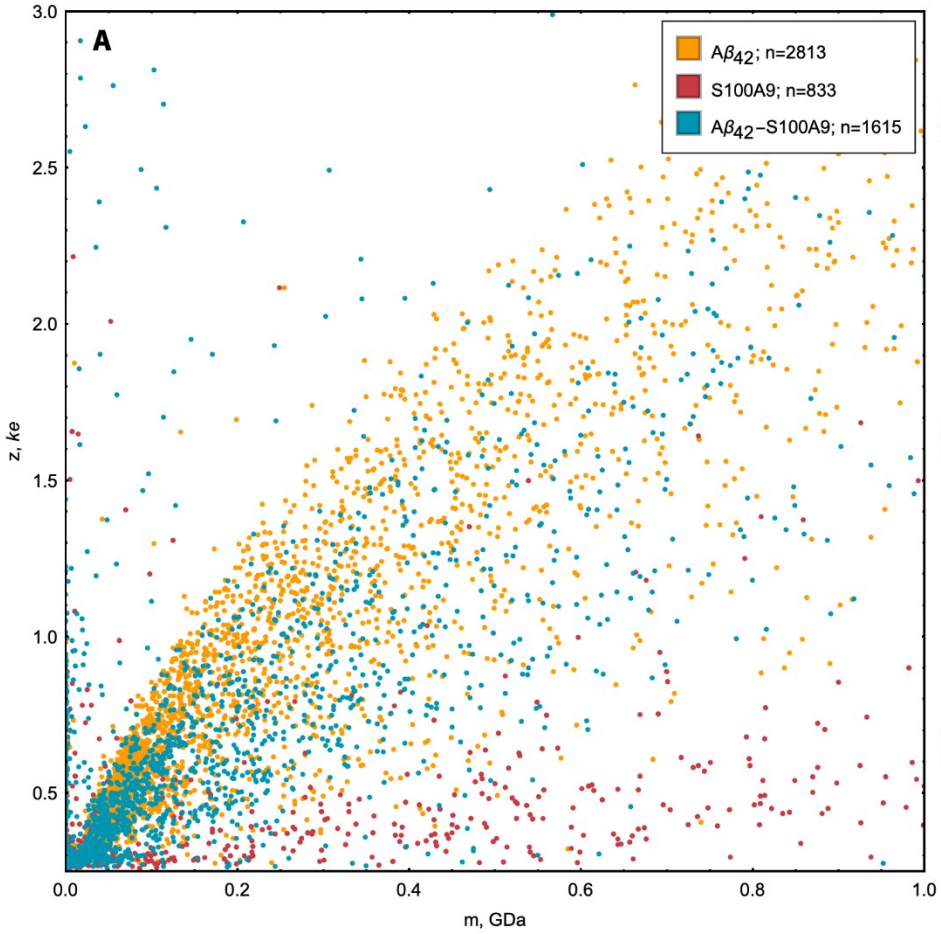

Figure S3. CDMS analysis of the amyloid samples. CDMS populations of amyloid particles with corresponding molecular masses (*m*) and charges (*z*) for the amyloid samples of $A\beta_{42}$ (in yellow), S100A9 (in red) and $A\beta_{42}$-S100A9 (in blue), respectively.

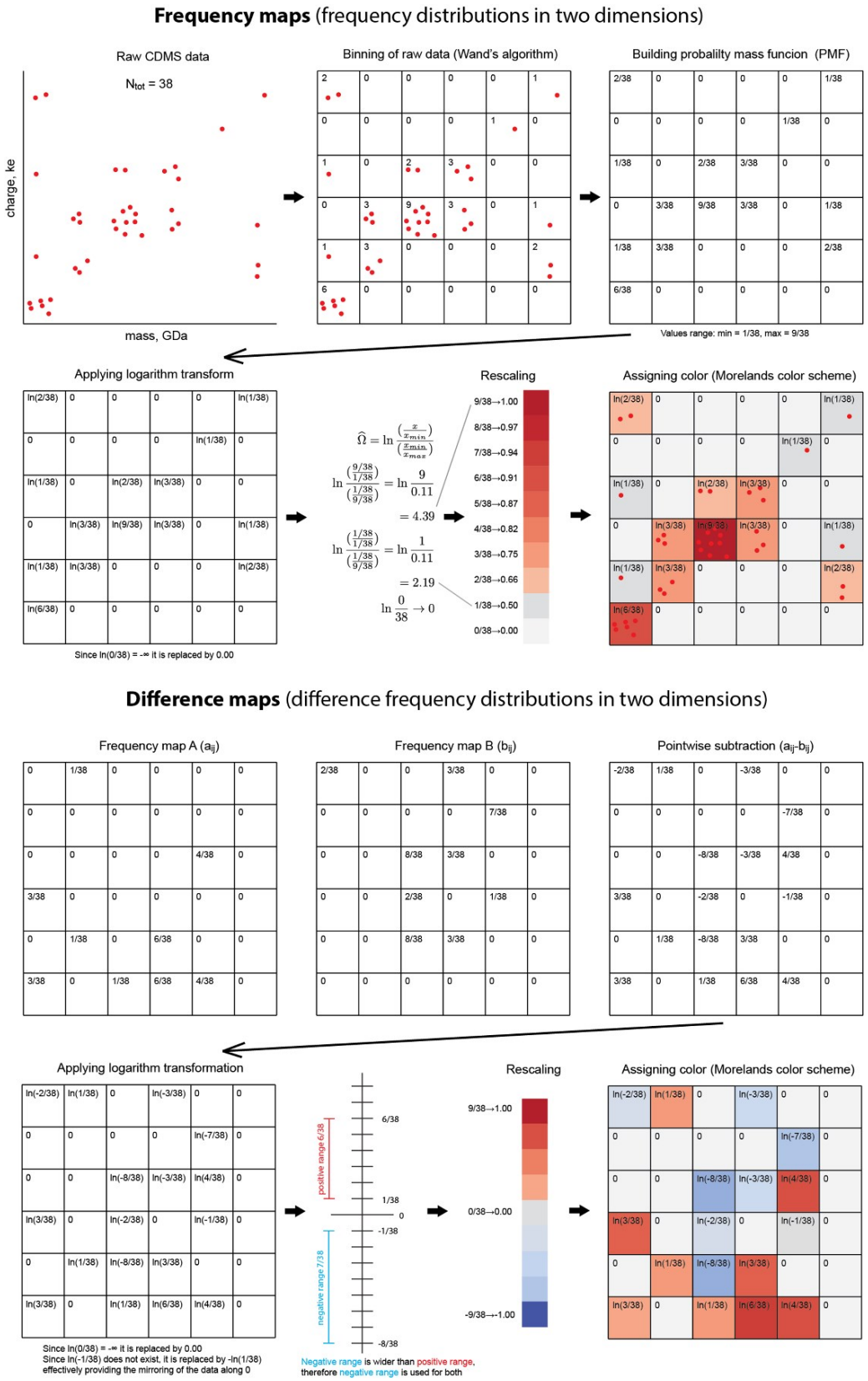

Fig. S4 Schematic presentation of the sequence of steps involved in calculation the CDMS frequency and differential maps, respectively

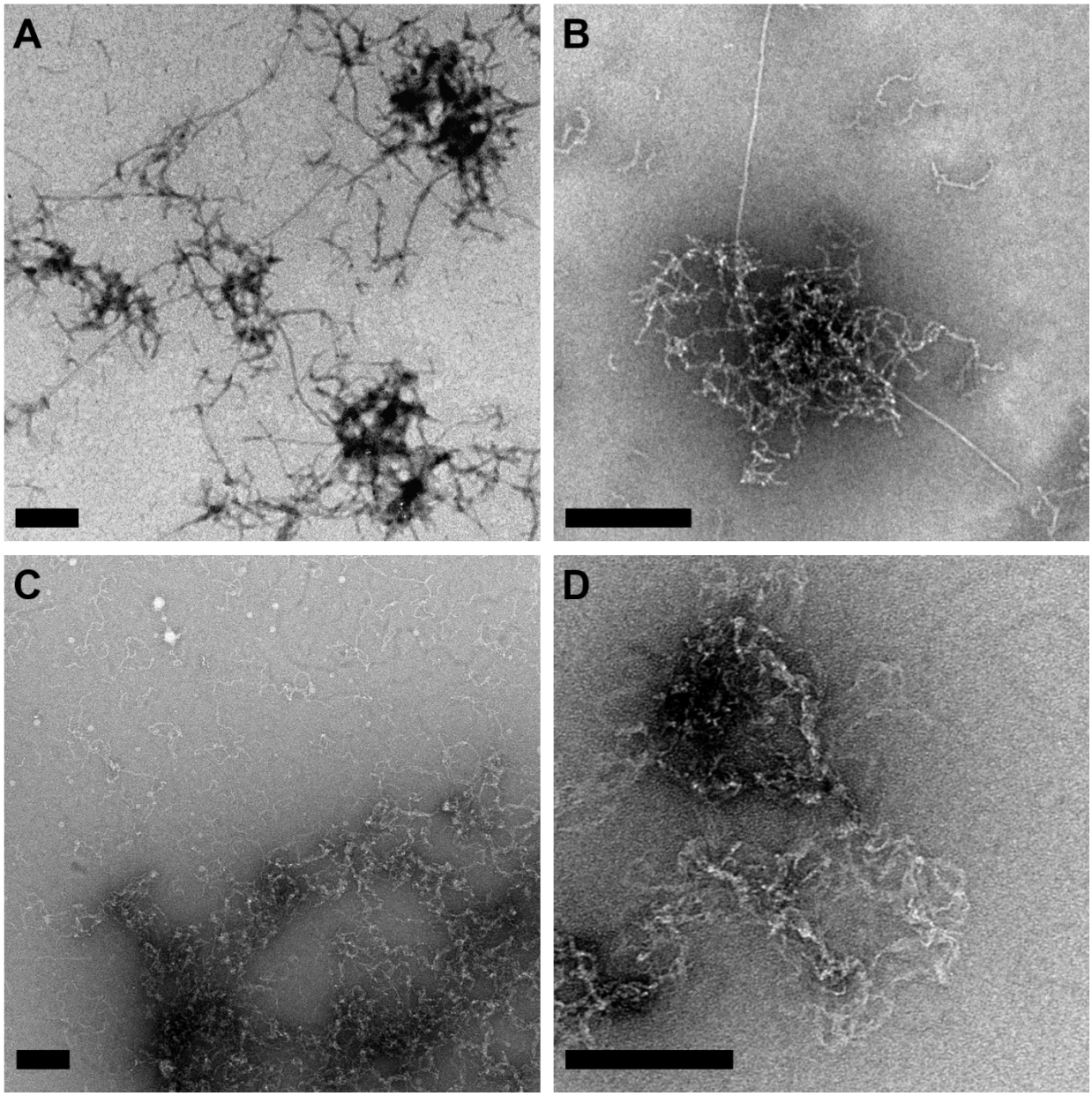

Figure S5. TEM images of $A\beta_{42}$ and S100A9 amyloids. (A,B) TEM images of $A\beta_{42}$ fibrils and their clusters presented at two magnifications. (C,D) TEM images of S100A9 amyloid fibrils and their coiling into amyloid clumps presented at two magnifications. Scale bars are 200 nm.

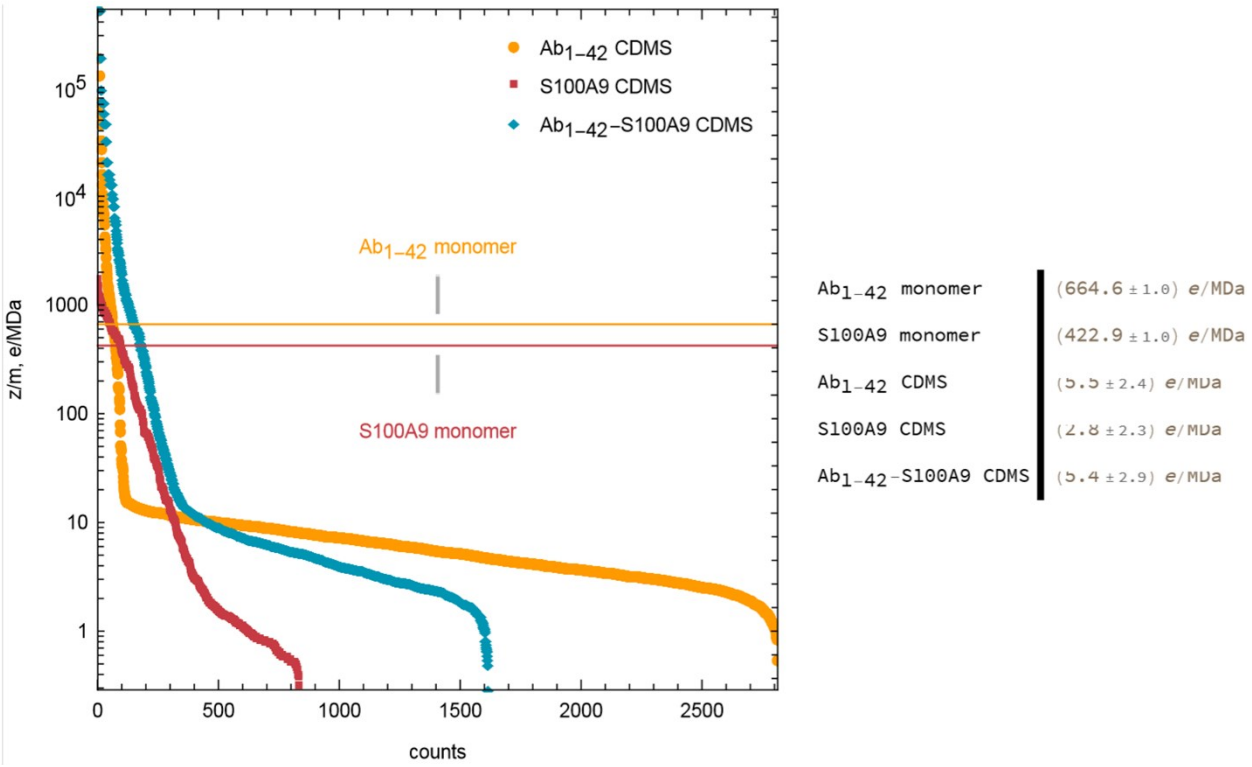

Figure S6. Ranking of amyloid particles according to their charge to mass ratio (*z/m*). Ratios of *z/m* of amyloid particles were taken from CDMS data and shown along *y*-axis. Positions of individual charged ions after their ranking are shown along *x*-axis. The ion positions corresponding to $A\beta_{42}$ fibrils are shown in yellow, for S100A9 fibrils – in red and for $A\beta_{42}$-S100A9 amyloids – in blue. *z/m* for $A\beta_{42}$ and S100A9 monomers were calculated by using their amino acid sequences at pH 7.4 and shown by horizontal lines in corresponding colours. The median values for each type of particles are indicated in figure legend.

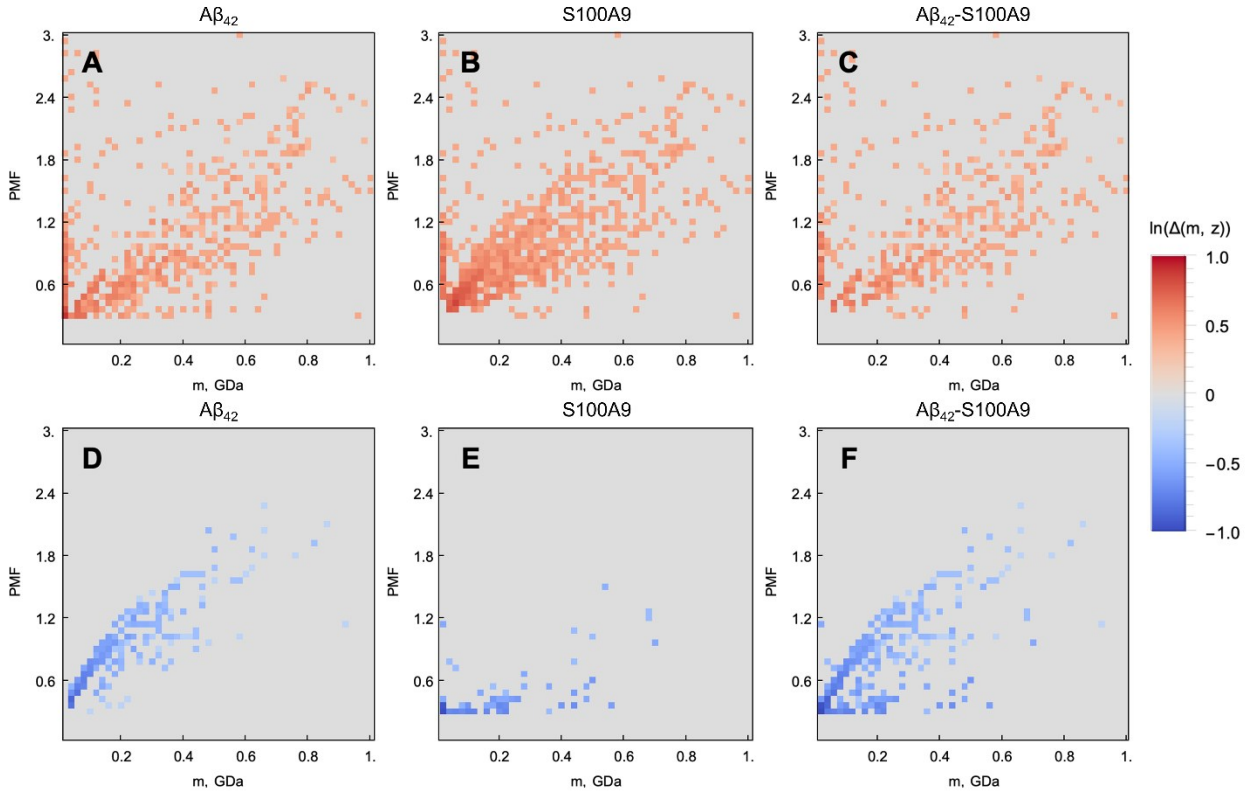

Figure S7. Difference maps derived by comparing CDMS data of Aβ$_{42}$-S100A9, Aβ$_{42}$ and S100A9 amyloid samples. Difference maps showing enriched populations of particles (in red) between the following amyloid samples: (A) Aβ$_{42}$-S100A9 and Aβ$_{42}$, (B) Aβ$_{42}$-S100A9 and S100A9 and (C) Aβ$_{42}$-S100A9 and Aβ$_{42}$ plus S100A9 samples filtered together, see ESI Material and Methods. Difference maps showing depleted populations of particles (in blue) between the following amyloid samples: (D) Aβ$_{42}$-S100A9 and Aβ$_{42}$, (E) Aβ$_{42}$-S100A9 and S100A9 and (F) Aβ$_{42}$-S100A9 and Aβ$_{42}$ plus S100A9 samples filtered together. The colour scales are shown on the right. 30 μM of each polypeptide were incubated individually or in mixture with each other for 24 h in PBS, pH 7.4 and 42°C.

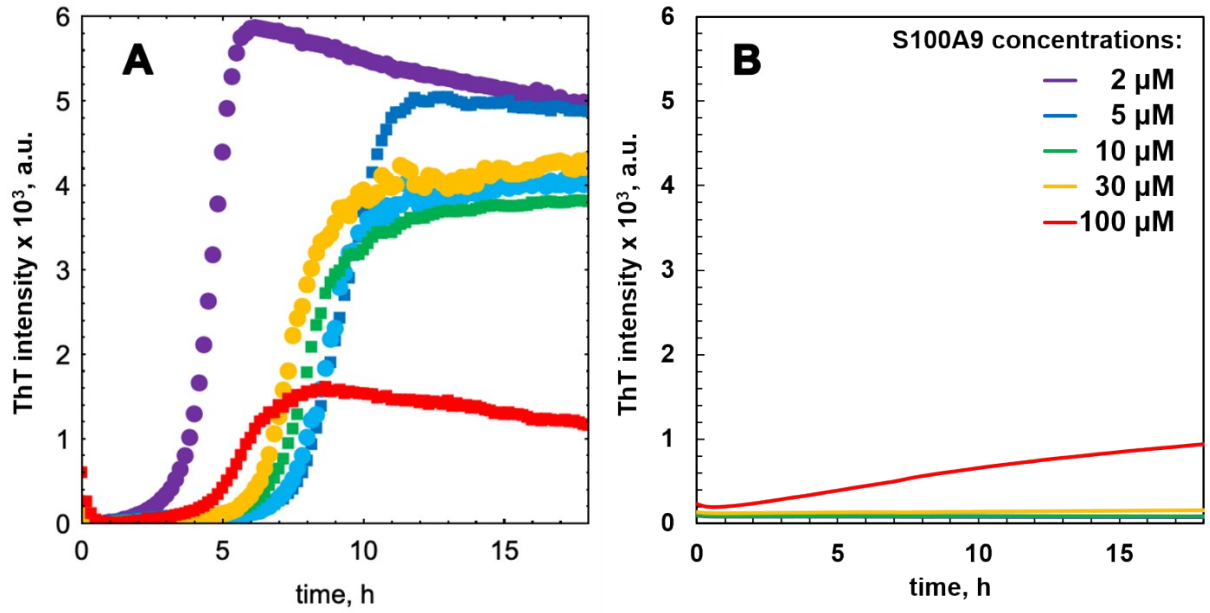

Figure S8. Amyloid fibrillation of $A\beta_{42}$, S100A9 and $A\beta_{42}$-S100A9 mixture monitored by ThT fluorescence assay. (A) Fibrillation kinetics of $A\beta_{42}$ and S100A9 mixtures monitored by ThT fluorescence. (B) Kinetics of S100A9 amyloid formation monitored at different concentrations as indicated in corresponding colour coding in the caption to Fig. 3B. 30 μM $A\beta_{42}$, PBS, pH 7.4 and 42°C.

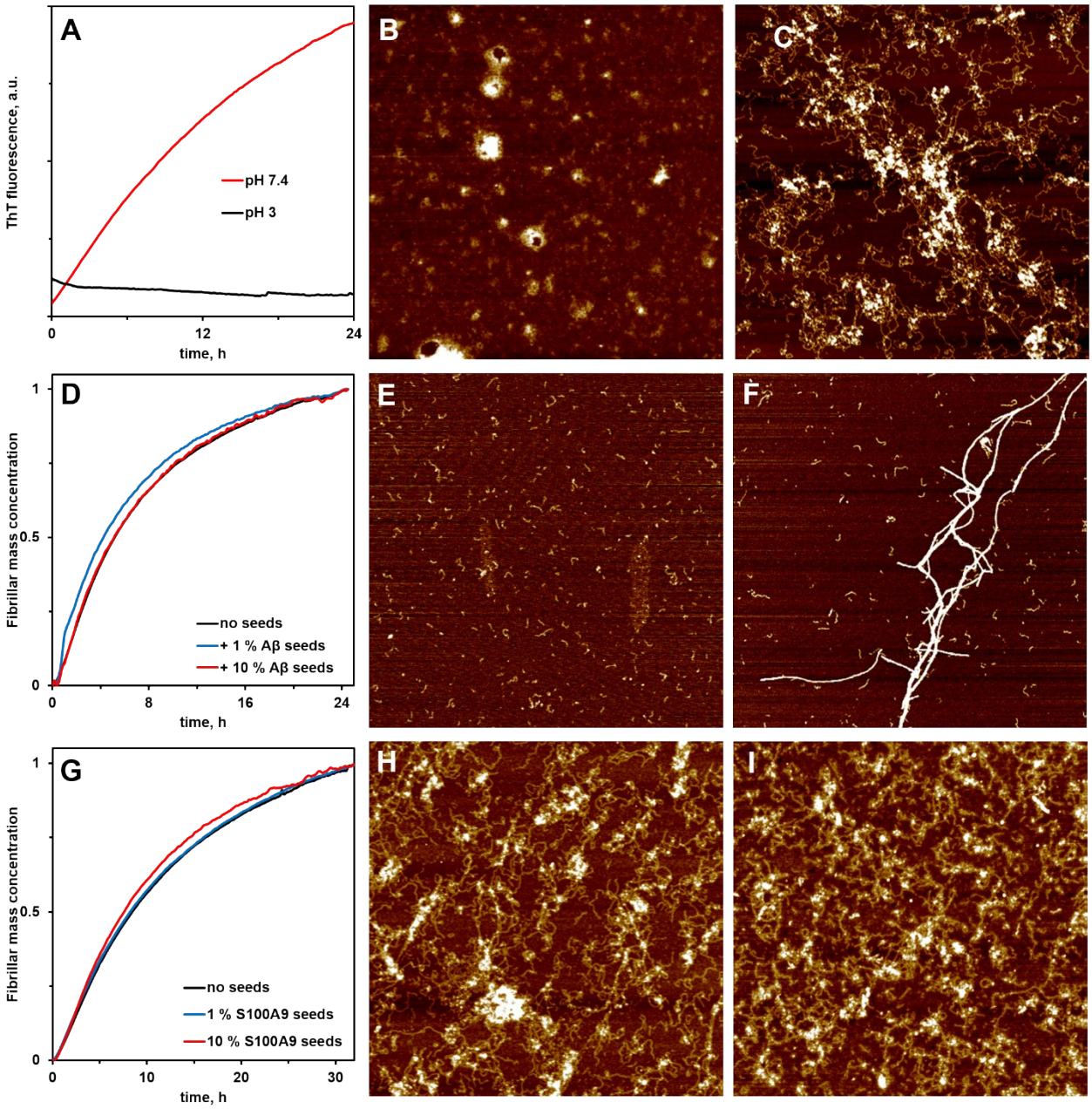

Figure S9. S100A9 does not form amyloids at pH 3 and its amyloids are not seeded by either its own seeds or $A\beta_{42}$ fibril cross-seeds. (A) S100A9 amyloid formation kinetics monitored by ThT fluorescence in 10 mM HCl, pH 3 (black line), PBS, pH 7.4 (red line) and 42°C. AFM images of (B) S100A9 aggregates observed at pH 3 and (C) pH 7.4 after 24 h incubation, 100 μM S100A9. (D) S100A9 amyloid formation kinetics monitored by ThT fluorescence in the absence (black line) and the presence of $A\beta_{42}$ seeds (in corresponding colours indicated in caption). 200 μM S100A9. AFM images of (E) 20 μM S100A9 in the absence and (F) in the presence of 2 μM $A\beta_{42}$ seeds after 8 h incubation. (G) S100A9 amyloid formation kinetics monitored by ThT fluorescence in the absence (black line) and the presence of S100A9 seeds (in corresponding colours indicated in caption). 100 μM S100A9. AFM images of (H) S100A9 in the absence and (I) in the presence of 10 μM S100A9 seeds after 24 h incubation. All experiments were carried out in PBS, pH 7.4 (except pH 3 condition) and 42°C. Scan sizes are 5 x 5 μm.

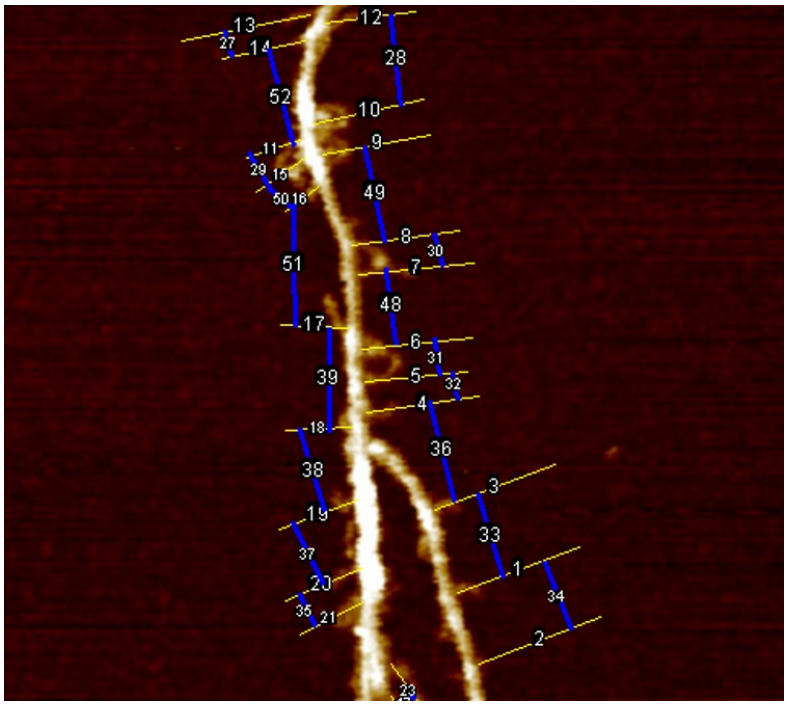

Figure S10. AFM measurements of the distances between S100A9 fibrils templated on the surface of $A\beta_{42}$-S100A9 amyloids. Representative AFM image of $A\beta_{42}$-S100A9 amyloid complex demonstrating the measurements of distances between templated S100A9 filaments. 30 μM of each polypeptide were co-incubated for 24 h in PBS, pH 7.4 and 42°C.

	$A\beta_{42}$	S100A9	$A\beta_{42}$–S100A9
Cumulative probability$_{m<0.08\ GDa}$ (4 of 50 bins)	0.37	0.45	0.43
Cumulative probability$_{z<0.36\ ke}$ (6 of 50 bins)	0.1	0.55	0.2

Table S1. Statistical analysis of CDMS experimental data.